Power Electronic Systems
Laboratory

IEEE Transactions on Power Electronics, Vol. 32, No. 4, pp. 2473-2480, April 2017

EMI Filter Volume Minimization of a Three-Phase, Three-Level T-Type PWM Converter System

D. O. Boillat,
F. Krismer,
J. W. Kolar

Eidgenössische Technische Hochschule Zürich
Swiss Federal Institute of Technology Zurich

Letters

EMI Filter Volume Minimization of a Three-Phase, Three-Level T-Type PWM Converter System

David Olivier Boillat, Florian Krismer, and Johann Walter Kolar

***Abstract*—In this study, the power density of a two-stage, i.e., $LCLCL$, electromagnetic interference (EMI) filter for a 10 kW three-phase, T-type three-level, boost-type PWM rectifier system is optimized concerning construction volume. It is found that reasonable boundary conditions limit or define most component values and only few degrees of freedom are remaining. In this context, the ratio of the first filter stage's common to differential mode inductance, $k_\mathrm{L} = L_\mathrm{cm,1}/L_\mathrm{dm,1}$, is identified to particularly affect the total filter volume. For given switching frequency and DC-link voltage of $f_\mathrm{s} = 48$ kHz and $V_\mathrm{dc} = 700$ V, a flat minimum of the overall filter volume results for $10 < k_\mathrm{L} < 40$. The boxed volume of the filter realized for $k_\mathrm{L} = 18$ is 763 cm^3 (46.6 in^3), which corresponds to a filter power density of 13.1 kW / dm^3 (215 W / in^3). Measurements of conducted EMI confirm that the rectifier system complies with the considered limits of conducted EMI (CISPR 11, class A).**

***Index Terms*—PWM converter, EMI filter, volume minimization, common mode, differential mode, CM choke, DM inductor.**

I. Introduction

RECENT publications reveal the suitability of mains-coupled T-type power converters for applications that demand a high power density, for example, in the field of inverters used in photovoltaic systems [1], [2] and battery chargers for electrical vehicles [3]. Because the electromagnetic interference (EMI) filter, needed in a mains-coupled power converter to sufficiently attenuate differential mode (DM) and common mode (CM) EMI noise [4], requires a substantial part of the total converter volume (typically around 30% of the total volume), a highly compact, i.e., optimized, realization of EMI filters is mandatory to achieve a high overall converter power density. In this context, this letter details a procedure for the volume-optimized design of the EMI filter of a three-phase, three-level T-type PWM rectifier stage, depicted in Fig. 1 and specified according to Table I, which forms the input stage of a controllable AC voltage source [5, 14].

Manuscript received July 25, 2016; revised September 15, 2016; accepted October 8, 2016. Date of publication October 12, 2016; date of current version January 20, 2017.

The authors are with the Power Electronic Systems Laboratory, Swiss Federal Institute of Technology Zurich, 8092 Zurich, Switzerland (e-mail: boillat@lem.ee.ethz.ch; krismer@lem.ee.ethz.ch; kolar@lem.ee.ethz.ch).

Color versions of one or more of the figures in this paper are available online at http://ieeexplore.ieee.org.

Digital Object Identifier 10.1109/TPEL.2016.2617085

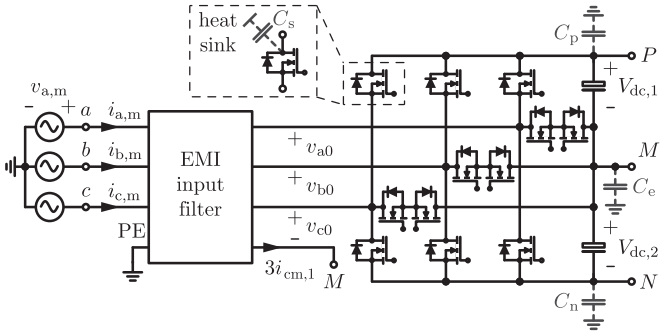

Fig. 1. Bidirectional three-phase, three-level PWM boost rectifier system with an EMI input filter.

TABLE I
Electrical Specifications of the Bidirectional Three-Phase PWM Boost Rectifier System Shown in Fig. 1

Nominal power P_nom	10 kW
Line-to-line mains rms voltage	400 V ($+10\%, -14\%$ [11])
Nominal current I_nom (rms value)	14.5 A
Maximum current I_max (rms value) [1)]	17 A
Nominal dc-link voltage $V_\mathrm{dc,nom}$	700 V
Mains frequency f_m	50 Hz
Switching (carrier) frequency f_s	48 kHz

1) The maximum current is obtained for $P_\mathrm{nom} = 10$ kW and for a mains voltage which is 14% lower than the nominal value.

Different filter optimization procedures are discussed in the literature, e.g., with respect to minimal weight [6], minimal harmonic distortion [7], or improved high-frequency (HF) behavior using an impedance-mismatch design technique [8]. With regard to this letter, the findings of [6], where a single-stage LC filter with a single filter choke (the DM inductance is integrated into the CM inductor) is investigated for a 5 kW / 208 V three-phase rectifier switching at 5 kHz, are particularly interesting: it identifies, with respect to minimal weight of the integrated choke, an optimal CM inductance to DM inductance ratio of 37. For a defined attenuation, however, the volume of a single-stage filter is considerably larger than the volume of a two-stage filter, cf., [9, pp. 400–403]. For this reason, in industrial applications, two-stage filters are of high interest.

Two-stage filters offer a high degree of freedom and a full optimization would be a computationally intensive task. However,

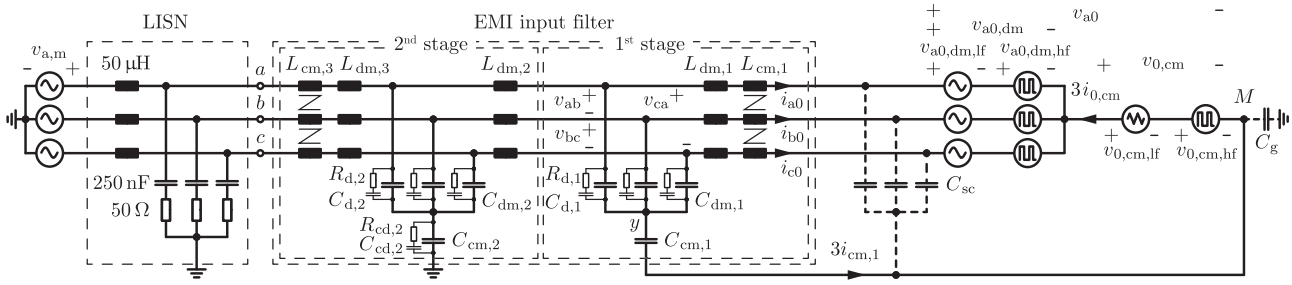

Fig. 2. Equivalent circuit of the three-phase rectifier system of Fig. 1 and proposed two-stage EMI filter structure. $C_{sc} = 2C_s = 267$ pF and $C_g = C_p + C_n + C_e = 25$ nF denote parasitic capacitances; $i_{cm,1,lf} \approx i_{0,cm,lf}$ is assumed. A carrier-based sinusoidal modulation with a superimposed zero-sequence component $v_{0,cm,lf} = -\left[\max\left(v_{a0,dm,lf}, v_{b0,dm,lf}, v_{c0,dm,lf}\right) + \min\left(v_{a0,dm,lf}, v_{b0,dm,lf}, v_{c0,dm,lf}\right)\right]/2$ is employed.

most component values are bound to technical side conditions, e.g., required attenuations, touch current limitation, etc., and this letter identifies the ratio of CM inductance to DM inductance of the first filter stage, k_L, to essentially remain as degree of freedom for optimization.

Based on initial investigations of the authors [10], the complete filter design procedure and experimental verification is discussed in the following. Section II-A describes the structure of the employed EMI filter, Sections II-B and II-C detail the used inductor models, and Section III summarizes the filter design and optimization procedure. Section IV verifies the optimized filter based on experimental results obtained from a 10 kW hardware prototype, which is operated according to Table I. The realized filter achieves a boxed volume of 763 cm^3, which corresponds to a filter power density of 13.1 kW/dm^3.

II. Filter Structure and Components

A. Filter Structure

Fig. 2 depicts the equivalent circuit of the three-phase rectifier system's power stage, the considered structure of the two-stage EMI filter, and the line impedance stabilization network (LISN). The power stage is replaced by low-frequency (LF) and HF CM and DM voltage sources, $v_{0,cm,lf}$, $v_{0,cm,hf}$, $v_{i0,dm,lf}$, and $v_{i0,dm,hf}$, with $i = a, b, c$. The heat sink is connected to the midpoint of the DC link M (cf., Fig. 1), offering a low impedance return path for the HF CM currents, which increases the achievable CM attenuation, and hence, allows potentially a more compact filter realization [12].

The first filter stage mainly requires boost (DM) inductors and DM capacitors, $L_{dm,1}$ and $C_{dm,1}$, and the CM filter components $L_{cm,1}$ and $C_{cm,1}$, where the CM capacitor is connected to the midpoint M, instead of earth, and feeds the CM current $3i_{cm,1}$ back to M (cf., Fig. 1) [13]. Due to this, the capacitance value of $C_{cm,1}$ can be selected without being constrained to $C_{cm,1} \leq 31$ nF [14] by reason of the maximum allowed touch current ($\sim$ earth current) of 3.5 mA according to EN 60335-1. This property facilitates a reduction of $L_{cm,1}$, widens the design-space available for filter optimization, and is found to allow for a more steady DC potential at the midpoint M, i.e., compared to the classical approach where $C_{cm,1}$ is connected between y and PE, the ripple of the voltage across C_e in Fig. 1 can be substantially reduced by a factor of up to 2–4, as can be shown by a more detailed analysis.

The second stage of the EMI filter employs DM inductors and DM capacitors and a CM capacitor; the DM inductors form the CM inductor, according to $L_{dm,2}/3 = L_{cm,2}$, in order to avoid the extra space needed for an explicit CM inductor and the introduction of additional (capacitive) parasitic couplings between the components. The filter further employs DM and CM inductors on the mains side, $L_{dm,3}$ and $L_{cm,3}$, which facilitate a reduction of the volume of the second filter stage and provide minimal inductances at the interface to the mains in order to prevent resonance phenomena in case of small inner mains impedances (stiff mains). Both filter stages use damping networks (series connections of resistors and capacitors) to provide attenuations at the resonance frequencies.

Besides passive filter concepts, the literature also reveals numerous active concepts, which allow for the compensation or filtering of CM noise in three-phase systems. Prominent examples include the injection of a CM compensation current [15], the use of a fourth bridge-leg to actively provide zero CM voltage at the inverter's output [16], and the use of CM chokes with four windings [17]. However, e.g., for [15], a linear amplifier stage is needed to generate the compensation current and for the system described in [16], the freewheeling states cannot be used and the modulation index is limited to 66%; active CM filters with a four-winding CM choke require a separate power stage [17]. This increase of the system complexity may often outweigh the potential benefits and accordingly to the best knowledge of the authors only passive EMI filters are employed in state-of-the-art industry applications. For this reason, the focus of this paper is on the optimization of passive EMI filters.

B. CM Inductor Modeling

The CM chokes are realized with toroidal tape-wound cores made of a high permeability nanocrystalline material (VITROPERM from VAC [18]). The CM inductance $L_{cm,1}$ of a symmetrical three-phase CM choke is [19]

$$L_{cm,1} = L_{choke,1}\,\frac{1 + 2k_{cm,1}}{3}, \qquad k_{cm,1} = \frac{L_{choke,1} - L_{\sigma,1}}{L_{choke,1}} \quad (1)$$

where $k_{cm,1}$ is the coupling factor, and $L_{choke,1}$ and $L_{\sigma,1}$ are self-inductance and leakage inductance of one phase winding, respectively.

The core losses P_{fe} are computed with the improved Generalized Steinmetz Equation (iGSE) [20], which is evaluated for the flux density waveform of the major loop (containing the frequency components at f_{m} and $3f_{\text{m}}$) and the minor loop (at f_{s}) [21]. To obtain the total core losses, the results of the iGSE for both loops are summed up.

The calculation of the copper losses P_{cu} takes skin and proximity effects according to [21] into account. The external magnetic field magnitude $H_{\text{ext,h}}$ at an inspected radius r generated by a certain CM current harmonic $i_{0,\text{cm,h}}$, needed to determine the proximity losses, is approximated with

$$H_{\text{ext,h}}(r) \approx \frac{3N\,|i_{0,\text{cm,h}}|\,/2}{l_{\text{circum}}(r)\;(\phi_{\text{w}}/120\,^\circ)} \tag{2}$$

where $l_{\text{circum}}(r)$ is the circumference around the choke and $\phi_{\text{w}} = 90^\circ$ is the angle over which one winding spreads out. To simplify the loss calculation, the magnetic field in the cross section of each conductor is assumed to be homogeneous with the magnitude being equal to $H_{\text{ext,h}}(r)$ at the center of the considered conductor. A comparison of the losses determined with the use of (2) and 2-D finite element method (FEM) simulations show a maximum relative error of 7%, and thus, confirm the practical applicability of (2).

A simple thermal model for passive cooling

$$T_{\text{choke}} \approx R_{\text{th}}\,(P_{\text{cu}} + P_{\text{fe}}) + 40\,^\circ\text{C} \leq 120\,^\circ\text{C},$$
$$R_{\text{th}} = \underbrace{\left[24\left(\frac{V_{\text{eff}}}{1\ \text{cm}^3}\right)^{-0.49}\right]}_{\text{fitted from [22]}} \text{(in the style of [23])}, \tag{3}$$

is employed in order to exclude unsuitable designs; V_{eff} is the effective magnetic core volume. If the temperature is less than $120\,^\circ$C, to reduce the volume, the wire diameter is reduced until $T_{\text{choke,max}} \approx 120\,^\circ$C applies. This thermal model is verified for the employed CM chokes in Section IV.

C. DM Inductor Modeling

Powder E-cores from Magnetics® (Kool Mμ® material [24]) are used for the DM inductors, due to their soft saturation characteristics and the absence of a concentrated air gap. In order to appropriately utilize the core material, at the peak current, a reduction of the inductance to 40% of the value at zero current is allowed. The optimization algorithm employed in Section III-A takes the implications of the nonlinear inductance on the bridge-leg input current ripple into account.

The calculation of the losses is similar to Section II-B: Core losses are calculated with the iGSE for major (at f_{m}) and minor loops (at f_{s}) and the calculation of the copper losses considers skin and proximity effects according to [21] with the average external magnetic field for E-cores being determined with the conductor mirroring approach as, for example, presented in [25]. Compared to 2-D FEM simulations, the maximum relative error with this method is 6%.

The maximum temperature of the DM inductor is assessed according to [24] for passive cooling

$$T_{\text{coil}} \approx \left(\frac{(P_{\text{cu}} + P_{\text{fe}})\,/1\ \text{mW}}{A_{\text{coil}}/1\ \text{cm}^2}\right)^{0.833} + 40\,^\circ\text{C} \leq 120\,^\circ\text{C}, \tag{4}$$

where A_{coil} is the open surface area of the inductor, i.e., the outer surface without the bottom surface. If the temperature is less than $120\,^\circ$C, to reduce the volume, the wire diameter is reduced until $T_{\text{coil,max}} \approx 120\,^\circ$C applies.

III. Optimized Filter Design

A. Optimization of the First Filter Stage

Initial circuit simulations reveal that the total required DM and CM attenuations (to fulfill CISPR 11, class A) are $\text{Att}_{\text{dm}} = 90$ dB and $\text{Att}_{\text{cm}} = 85$ dB at $f = 192$ kHz, respectively. Due to the approximately rectangular waveforms of the switched voltages, the envelopes of the spectra of conducted EMI noise are approximately proportional to $1/f$, cf., [26]. Within the frequency band specified in CISPR 11, $150\,\text{kHz} \leq f \leq 30\,\text{MHz}$, the greatest noise amplitudes are thus expected for the spectral EMI noise components at 4×48 kHz $= 192$ kHz. The partitionings of the total DM and CM attenuations among the two filter stages represent two degrees of freedom in the filter design. In a first step, the attenuations of the first filter stage are set to $\text{Att}_{1,\text{dm}} = 45\,\text{dB} = 90\,\text{dB}/2$ and $\text{Att}_{1,\text{cm}} = 60\,\text{dB} > 85\,\text{dB}/2$ in order to obtain reasonable values of the peak-to-peak voltage ripples of $6\% \times (\sqrt{2} \times 230\ \text{V})$ for the DM and the CM capacitors (an increased CM attenuation is selected for the first filter stage, since $C_{\text{cm,1}}$ is not restricted by means of a limited touch current, and hence, directly allows reducing the inductance value of $L_{\text{cm,3}}$). It is typically avoided to further lower the attenuation Att_1 of the first filter stage, as this would lead to a higher attenuation Att_2 of the second stage, which would implicate physically larger components with higher parasitic component values and unfavorable HF properties, i.e., an undesired reduction of the attenuation at higher frequencies. With regard to increased values of $\text{Att}_{1,\text{dm}}$, an in-depth optimization reveals that a marginal reduction of the total filter volume by maximum 3% is achievable for $\text{Att}_{1,\text{dm}} = 50$ dB.[1] Regarding CM, for an attenuation of the first filter stage of $\text{Att}_{1,\text{cm}} = 78$ dB, $L_{\text{cm,3}}$ (cf., Section III-C) can be omitted, and hence, the boxed volume of the entire filter would be reduced to 380 cm^3, which is only 5% lower than 400 cm^3. However, during the process of investigations, it has been found that parasitics of the hardware setup already reduce the achieved CM attenuation of the first stage from 60 dB to 50 dB (for the selected design, cf., Table III) and would lead to even a larger attenuation reduction for $\text{Att}_{1,\text{cm}} = 78$ dB. Thus, the initially proposed partitioning of the attenuation among the two filter stages is found to represent an almost optimal choice and a very suitable starting point for a first design iteration.

Table II summarizes further assumptions and boundary conditions. In order to avoid unwanted increases of the phase rms currents and to enable sufficiently accurate current measurements,

[1]For DM attenuations $\text{Att}_{1,\text{dm}} = \{45\,\text{dB}, 50\,\text{dB}, 55\,\text{dB}\}$, the calculated total filter volumes (first plus second filter stages) are $V_{\text{tot}} = \{400\ \text{cm}^3, 388\ \text{cm}^3, 457\ \text{cm}^3\}$, respectively.

TABLE II
MAXIMUM ALLOWED VALUES OF ELECTRIC, MAGNETIC, AND THERMAL PARAMETERS EMPLOYED FOR THE MINIMIZATION OF THE VOLUME OF THE FIRST EMI FILTER STAGE AND PARAMETER VALUES OBTAINED FROM THE VOLUME-OPTIMIZED DESIGN (CF TABLE III); $V_{\mathrm{M,PK}} = \sqrt{2} \times 230$ V, $I_{\mathrm{NOM,PK}} = \sqrt{2} \times 14.5$ A

No.	Parameter	Boundary Value	Selected Design Value
1(a)	Peak-to-peak bridge-leg input current ripple at zero current	$25\% \times I_{\mathrm{nom,pk}}$	$25\% \times I_{\mathrm{nom,pk}}$
1(b)	Peak-to-peak bridge-leg input current ripple due to no. 8	$60\% \times I_{\mathrm{nom,pk}}$	$49\% \times I_{\mathrm{nom,pk}}$
2	Peak-to-peak DM voltage ripple across $C_{\mathrm{dm,1}}$	$6\% \times V_{\mathrm{m,pk}}$ [1)]	$6\% \times V_{\mathrm{m,pk}}$ [1)]
3	Peak-to-peak CM voltage ripple across $C_{\mathrm{cm,1}}$	$6\% \times V_{\mathrm{m,pk}}$ [1)]	$6\% \times V_{\mathrm{m,pk}}$ [1)]
4	Amplitude of LF current through $C_{\mathrm{dm,1}}$	max. $1\% \times I_{\mathrm{nom,pk}}$	$0.6\% \times I_{\mathrm{nom,pk}}$
5	Amplitude of LF current through $C_{\mathrm{cm,1}}$	max. $1\% \times I_{\mathrm{nom,pk}}$	$0.03\% \times I_{\mathrm{nom,pk}}$
6	Peak flux density, CM inductor	max. $70\% \times 1.2$ T	$63\% \times 1.2$ T
7	Peak flux density, DM inductor	max. 1 T	0.35 T
8	Permeability reduction, DM inductor	min. $40\% \times \mu_{\mathrm{i}}$ [2)]	$40\% \times \mu_{\mathrm{i}}$ [2)]
9	Temperature of CM inductor	max. 120 °C [3)]	118 °C [3)]
10	Temperature of DM inductor	max. 120 °C [3)]	119 °C [3)]
11	Angle ϕ_{w} which is covered by one CM choke's winding	90 °	90 °

The parameters take a variation of the mains voltage according to Table I into consideration. [1)] $6\% \times V_{\mathrm{m,pk}}$ corresponds to $3\% \times V_{\mathrm{dc,nom}}$; [2)] $\mu_{\mathrm{i}} =$ initial permeability, i.e. the permeability at zero current; [3)] ambient temperature $T_{\mathrm{a}} = 40\,^{\circ}\mathrm{C}$.

the bridge-leg input current ripple is limited to a peak-to-peak value of 5.1 A [$25\% \times (\sqrt{2} \times 14.5$ A), cf., Table I] at phase currents close to zero. The permeabilities of the DM inductors' powder cores are allowed to drop to 40% of their initial permeabilities (at zero current) for the maximum fundamental mains phase current ($\sqrt{2}I_{\mathrm{max}} = 24$ A) to better utilize the magnetic material, which could lead to a maximum peak-to-peak current ripple of $(25\%/40\%) \times (\sqrt{2} \times 14.5\ \mathrm{A}) = 63\% \times (\sqrt{2} \times 14.5\ \ \mathrm{A}) \approx 60\% \times (\sqrt{2} \times 14.5\ \ \mathrm{A}) = 51\% \times (\sqrt{2} \times 17\ \ \mathrm{A})$. Furthermore, the rms currents through $C_{\mathrm{dm,1}}$ at f_{m} and $C_{\mathrm{cm,1}}$ at $3f_{\mathrm{m}}$ are limited to $1\% \times 14.5$ A, to prevent a significant increase of the rms currents of the power stage. The maximum surface temperatures are limited to $120\,^{\circ}\mathrm{C}$ at operation under worst-case conditions, i.e., with maximum phase current of 17 A (cf., Table I).

Since the first filter stage in principle enables the use of low CM inductance values, relatively high CM currents could occur. For this reason, the peak-to-peak input current ripple is obtained from the superposition of the phase current's DM and CM components. From direct deductions — a small CM inductance leads to a great CM current ripple, and thus, the DM inductors need to be increased and vice versa — it remains open, how to best select $L_{\mathrm{cm,1}}$ and $L_{\mathrm{dm,1}}$ to achieve minimum filter volume. The corresponding degree of freedom, e.g., the value of $L_{\mathrm{cm,1}}$, is advantageously expressed with the inductance ratio $k_{\mathrm{L}} = L_{\mathrm{cm,1}}/L_{\mathrm{dm,1}}$.

Based on these considerations, the first filter stage is optimized with the procedure listed as follows:

1) initiate $L_{\mathrm{cm,1,tot}}$ according to a geometric series, $L_{\mathrm{cm,1,tot}} = 100\ \mu\mathrm{H} \times 10^{(i/16)}$; i is the loop counter, $5 < i < 36$, $i \in \mathbb{N}$;
2) compute $L_{\mathrm{dm,1,tot}}$ for the given phase current ripple at zero current;
3) compute $C_{\mathrm{dm,1}}$ and $C_{\mathrm{cm,1}}$ for the given voltage ripples;
4) design of the CM choke, $L_{\mathrm{cm,1}} = L_{\mathrm{cm,1,tot}} - L_{\mathrm{dm,1,tot}}/3$;
5) design of the DM inductor, $L_{\mathrm{dm,1}} = L_{\mathrm{dm,1,tot}} - L_{\sigma,1}$.

The damping elements $C_{\mathrm{d,1}}$ and $R_{\mathrm{d,1}}$ are designed for $C_{\mathrm{d,1}}/C_{\mathrm{dm,1}} = 0.25$ and a maximum resonant gain of 20 dB.

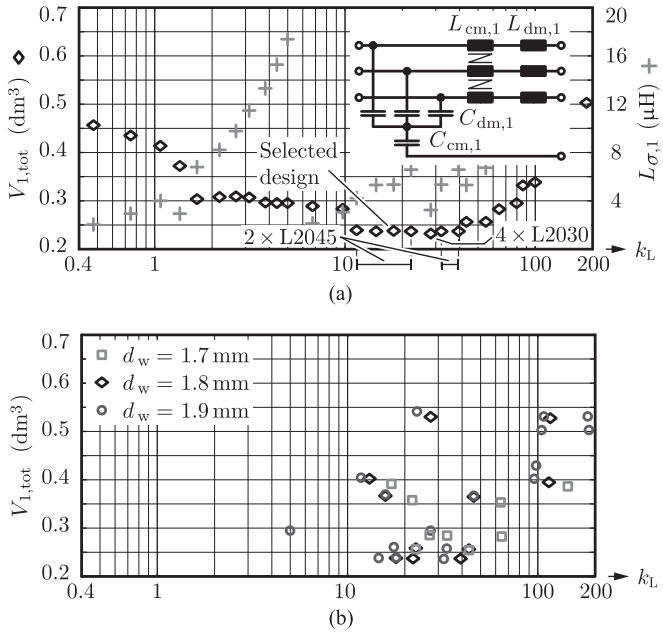

Fig. 3. (a) Total boxed volume $V_{1,\mathrm{tot}} = 3V_{\mathrm{L,dm,1}} + V_{\mathrm{L,cm,1}} + 3V_{\mathrm{C,dm,1}} + V_{\mathrm{C,cm,1}}$ (volumes of the damping elements neglected) of the first EMI filter stage and leakage inductance $L_{\sigma,1}$ of $L_{\mathrm{cm,1}}$, evaluated for different values of $k_{\mathrm{L}} = L_{\mathrm{cm,1}}/L_{\mathrm{dm,1}}$ computed with the algorithm presented in Section III-A. (b) $V_{1,\mathrm{tot}}$ calculated with the practical approach as explained in Section III-B for a enameled wire diameter of $d_{\mathrm{w}} = 1.7$ mm, 1.8 mm, and 1.9 mm.

B. Optimization Result Discussion

Fig. 3(a) depicts the boxed filter volumes for different values of k_{L} obtained for the boundary conditions listed in Table II and reveals that a flat minimum results for $10 < k_{\mathrm{L}} < 40$. The minimum occurs for $k_{\mathrm{L}} = 28$; this solution, however, requires a realization of the CM choke with four stacked cores and features only a slightly smaller filter volume than the surrounding solutions. The remaining results for $10 < k_{\mathrm{L}} < 40$ consider two stacked cores with same physical dimensions (T60006-L2045 by VAC) and core materials with different permeabilities (V101, V102, and V118 material specifications [18]). However, some

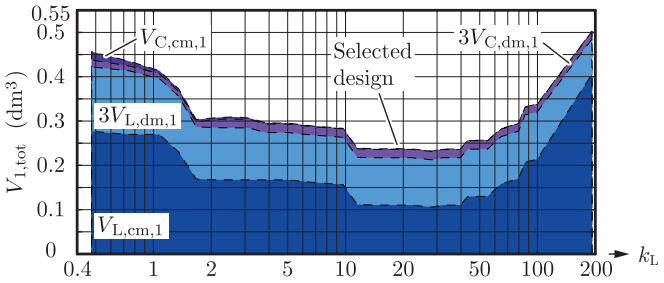

Fig. 4. Total boxed volume $V_{1,\mathrm{tot}}$ of the first filter stage and its partitioning into the corresponding boxed volumes of the individual components over $k_\mathrm{L} = L_{\mathrm{cm},1} \,/\, L_{\mathrm{dm},1}$ [damping elements neglected, cf., Fig. 3(a)].

of the obtained results employ a reduced number of turns to reduce the inductance obtained with the considered high permeability ring cores, which cannot implement air gaps, and thus, do not fully exploit the available winding area (still, $V_{1,\mathrm{tot}}$ is close to the minimum, because, for the investigated system and $2 < k_\mathrm{L} < 100$, a decrease of $L_{\mathrm{cm},1}$ causes only a marginal increase of $L_{\mathrm{dm},1}$).

Based on this consideration, an alternative, more practical, approach has been developed to verify the obtained result: for a given wire diameter $d_{\mathrm{w},i}$ and CM choke core Core$_i$, the maximum number of turns N_i, that fit on the core, is calculated, and in case of core saturation, n_i cores are stacked to avoid saturation (up to five, otherwise the core is not considered). Therefore, a preliminary CM choke design, with N_i, n_i, and $d_{\mathrm{w},i}$, exists for each considered Core$_i$, for which the other filter component values are computed and the DM inductor can be designed. In a final step, simulated current and voltage waveforms are used to test the preliminary design against the boundary conditions of Table II. Fig. 3(b) depicts the results obtained with this practical approach, for $d_\mathrm{w} = 1.7$ mm, 1.8 mm, and 1.9 mm (maximum current densities in 6.0 A/mm^2 ... 7.5 A/mm^2; $d_\mathrm{w} = 1.8$ mm has been identified to lead to the minimal boxed volumes of the first filter stage). Both procedures identify the same results with respect to minimum filter volume and a flat optimum results for $10 < k_\mathrm{L} < 40$.

From the results depicted in Fig. 3(a), $k_\mathrm{L} = 18$ has been selected for the realization. This design features a practically reasonable CM inductor with two stacked cores and employs the core material V118 ($k_\mathrm{L} = 18$ and 22), which, together with the core material V101 ($k_\mathrm{L} = 12$ and 15), features less reduction of permeability at higher frequencies than the material V102 ($k_\mathrm{L} = 32$ and 40). The optimization procedure minimizes the inductor volumes with respect to the specified thermal limitations, given in Table II, and for this reason, the maximum inductor temperatures (118 °C and 119 °C) are close to the limit of 120 °C. Moreover, the allowable reduction of the permeability of the DM inductor's core is fully utilized, which, for the given powder core material (KoolMμ® 60μ), translates to a maximum allowed magnetic field density of 0.35 T, and for the given value of k_L, leads to a maximum relative peak-to-peak bridge-leg input current ripple of 49%. For the CM choke, the maximum flux density is close to the allowed maximum (condition 6 in Table II). The optimized filter design considers capacitors, which fully utilize the maximum specified values of the HF

TABLE III
OPTIMIZATION RESULT OBTAINED FOR THE CONSIDERED EMI FILTER AND DETAILS RELATED TO THE FINAL HARDWARE REALIZATION

Comp.	Design Value	Hardware Realization
$L_{\mathrm{dm},1}$	163.5 μH	Four stacked E-cores (00K3007E060, Magnetics®), $N = 25$, $d_{\mathrm{cu}} = 1.4$ mm (enameled wire)
$C_{\mathrm{dm},1}$	850 nF	1.0 μF||4.7 nF* (B32923C3105K, EPCOS; 502S47W472KV3E-SC, Johanson Dielect.)
$L_{\mathrm{cm},1}$	2.94 mH	Two stacked toroidal cores (T60006-L2045-V118, VAC), $N = 9$, $d_{\mathrm{cu}} = 1.8$ mm (enameled wire)
$C_{\mathrm{cm},1}$	87 nF	100 nF||4.7 nF* (B32921C3104M, EPCOS; 502S47W472KV3E-SC, Johanson Dielect.)
$C_{\mathrm{d},1}$	212 nF	220 nF (B32923C3224M, EPCOS)
$R_{\mathrm{d},1}$	66.1 Ω	133 Ω||133 Ω (CRCW2512133RFKEGHP, Vishay)
$L_{\mathrm{dm},2}$	29 μH	Five stacked E-cores (00K2510E060, Magnetics®), $N = 10$, $d_{\mathrm{cu}} = 1.4$ mm (enameled wire)
$C_{\mathrm{dm},2}$	2.1 μF	2.2 μF||4.7 nF* (B32924C3225K, EPCOS; 502S47W472KV3E-SC, Johanson Dielect.)
$C_{\mathrm{cm},2}$	26 nF	22 nF||4.7 nF* (B32022B3223K, EPCOS; 502S47W472KV3E-SC, Johanson Dielect.)
$C_{\mathrm{d},2}$	517 nF	680 nF (B32924C3684K, EPCOS)
$R_{\mathrm{d},2}$	17.8 Ω	35.7 Ω||35.7 Ω (ERJ-1TNF35R7U, Panasonic)
$C_{\mathrm{cd},2}$	5 nF	4.7 nF (502S47W472KV3E-SC, Johanson Dielect.)
$R_{\mathrm{cd},2}$	199 Ω	390 Ω||390 Ω (1206 SMD chip resistors)
$L_{\mathrm{dm},3}$	11.7 μH	Two stacked E-cores (00K1808E060, Magnetics®), $N = 11$, $d_{\mathrm{cu}} = 1.4$ mm (enameled wire)
$L_{\mathrm{cm},3}$	2.0 mH	Toroidal core (T60006-L2030-W514, VAC), $N = 8$, $d_{\mathrm{cu}} = 1.4$ mm (enameled wire)

* The 4.7 nF ceramic capacitors improve the HF properties of the filter.

The sum of all components' boxed volumes is 400 cm^3.

CM and DM voltage ripples and realize LF capacitor currents that are below the set limits (for selected CM and DM capacitances, the HF and LF conditions are coupled, cf., conditions 2, 4 and 3, 5 in Table II for DM and CM, respectively).

Fig. 4 depicts the volumes of the different filter components for the k_L values given in Fig. 3(a). According to this result, the capacitors have a minor contribution to the total filter volume and the volume of the DM inductor slightly decreases for increasing values of k_L. However, the characteristic of the volume of the CM inductor mainly affects the characteristic of $V_{1,\mathrm{tot}}$ and two ranges of k_L can be distinguished: $k_\mathrm{L} < 10$ and $k_\mathrm{L} > 40$. For $k_\mathrm{L} < 10$, low values of $L_{\mathrm{cm},1}$, and due to the great A_L-values of the selected high permeability nanocrystalline cores, low numbers of turn result. Subsequently, large cores are needed to avoid saturation. For $k_\mathrm{L} > 40$, large inductor cores are required to achieve high CM inductance values, e.g., $L_{\mathrm{cm},1} = 15.0$ mH for $k_\mathrm{L} = 100$.

C. Second Filter Stage

A maximum total reactive current of $2\% \times 14.5$ A (at f_m) is defined for the DM capacitors of both filter stages. With this, the volumes of the capacitors are found to be less than the volumes of the inductors and minimum filter volume is obtained at the maximum tolerated reactive current. Thus, with $C_{\mathrm{d},1}/C_{\mathrm{dm},1} = C_{\mathrm{d},2}/C_{\mathrm{dm},2} = 0.25$, the values of all filter capacitors are defined, cf., Table III. $L_{\mathrm{dm},2}$ and $L_{\mathrm{dm},3}$ are selected such that all DM resonance frequencies of the filter are less than $90\% \times f_\mathrm{s}$ and for a DM attenuation of 40 dB. A simple volume optimization, based on the assumption that

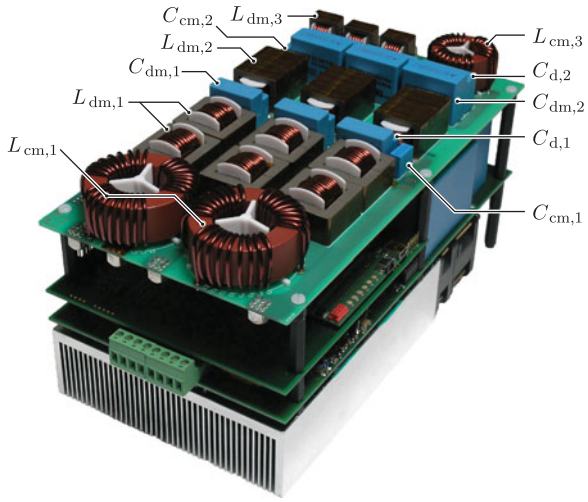

Fig. 5. Picture of the realized 10 kW hardware prototype employing SiC MOSFETs and featuring a bidirectional three-phase, three-level PWM rectifier, which supplies the four-phase, three-level output inverter stage presented in [5, 14]; the $LCLCL$ EMI filter according to the network of Fig. 2 is on top. Converter dimensions: 240 mm × 130 mm × 120 mm (length × width × height).

the inductor volume is proportional to the inductance, yields: $L_{\mathrm{dm},2,\mathrm{tot}} = 29\ \mu\mathrm{H}$ and $L_{\mathrm{dm},3,\mathrm{tot}} = 14\ \mu\mathrm{H}$.

The maximum total CM capacitance of the second filter stage is 31 nF in order to not exceed the maximum touch current, cf., Section II-A. Due to this limitation and with $C_{\mathrm{cd},2} = C_{\mathrm{cm},2}/5$, the capacitances $C_{\mathrm{cm},2} = 26\ \mathrm{nF}$ and $C_{\mathrm{cd},2} = 5\ \mathrm{nF}$ result. To avoid the introduction of additional parasitic, e.g., capacitive, coupling between the components no explicit CM choke is connected in series to $L_{\mathrm{dm},2}$, i.e., $L_{\mathrm{cm},2} = L_{\mathrm{dm},2,\mathrm{tot}}/3 = L_{\mathrm{dm},2}/3$ applies. Thus, $L_{\mathrm{cm},3}$ is designed such that the second filter stage (plus $L_{\mathrm{cm},3}$) achieves the required CM attenuation of 30 dB and $L_{\mathrm{cm},3} = 2.5 \times 0.8\ \mathrm{mH}$ results, which takes a safety factor of 2.5 into account to consider the reduced permeability of the selected nanocrystalline core material at 192 kHz.[2]

Table III lists all final results, which considers the interdependencies of the DM and CM inductors, due to the CM chokes' stray inductances and the DM inductors' effective CM inductances. The sum of all calculated boxed volumes is $400\ \mathrm{cm}^3$.

IV. Experimental Results

Fig. 5 depicts the realized 10 kW hardware prototype. The two-stage DM and CM EMI filter printed circuit board (PCB) is on top, with the first filter stage in the front. The realized filter achieves a boxed volume of $763\ \mathrm{cm}^3$, which is more than one and a half times the sum of the boxed volumes of all components ($483\ \mathrm{cm}^3$).[3] This ratio of realized to calculated (summed-up) volumes is addressed to neglected parts of the filter, here the PCB, and unusable space (air), which appears due to different (incompatible) physical dimensions of the filter's components and typically requires most of the additional volume. The realized filter volume represents roughly 20% of the entire converter volume of $3.74\ \mathrm{dm}^3$.

TABLE IV
Calculated and Measured Maximum Temperatures (At the Winding Surfaces) at $T_{\mathrm{AMB}} = 29\,^{\circ}\mathrm{C}$ for the Inductors Listed in Table III and for Nominal Operating Conditions

Inductor	Max. Meas. Temp.	Max. Calc. Temp.	Rel. Error
$L_{\mathrm{cm},1}$	$88.3\,^{\circ}\mathrm{C}$	$75.5\,^{\circ}\mathrm{C}$	21.6%
$L_{\mathrm{cm},3}$	$82.8\,^{\circ}\mathrm{C}$	$82.8\,^{\circ}\mathrm{C}$	0%
$L_{\mathrm{dm},1}$	$154.8\,^{\circ}\mathrm{C}$	$116.2\,^{\circ}\mathrm{C}$	30.7%
$L_{\mathrm{dm},2}$	$101.9\,^{\circ}\mathrm{C}$	$95.3\,^{\circ}\mathrm{C}$	9.1%
$L_{\mathrm{dm},3}$	$90.5\,^{\circ}\mathrm{C}$	$87.3\,^{\circ}\mathrm{C}$	5.2%

It is noted that, after the optimization was conducted, $L_{\mathrm{dm},1}$ has been realized with two inductors that are located close to each other in order to improve the boxed volume of the filter.

Table IV compares calculated to measured maximum temperatures at the surfaces of the inductors listed in Table III at nominal operating conditions. The measurements are conducted on the fully populated EMI filter PCB [the relative error is calculated with: $e_{\mathrm{rel}} = (T_{\mathrm{meas}} - T_{\mathrm{calc}})/(T_{\mathrm{meas}} - T_{\mathrm{amb}})$]. The simple temperature models achieve acceptable errors of less than 10% for the inductors of the second filter stage. However, the temperatures of the inductors of the first filter stage are underestimated by up to 31%, which is explained by the close proximities of $L_{\mathrm{cm},1}$ and $L_{\mathrm{dm},1}$. The maximum measured temperature for $L_{\mathrm{dm},1}$ is obtained for the coil in the middle of the PCB, which is completely surrounded by other heated up components (cf., Fig. 5). Furthermore, the calculated temperature of $L_{\mathrm{dm},1}$ takes the reduction of outer cooling surfaces available for natural convection due to the arrangement of $L_{\mathrm{dm},1}$ on the PCB (cf., Fig. 5) into account.[4] This has not been considered for the optimization; in contrast, in the course of the design, free space around the inductor was assumed.

In this context, more detailed thermal models, e.g., [27], would feature improved accuracy, at the cost of a higher computational effort. Furthermore, the inductive components could be placed in an air stream to reduce their maximum surface temperatures. This, however, would require the use of an additional fan or a redesign of the converter, since the actual arrangement of the filter board is on top of the converter (cf., Fig. 5).

Fig. 6 compares the calculated filter transfer functions (DM and CM) to the measured transfer functions. The calculated transfer functions employ the network of Fig. 2 and the component values measured at $f = f_{\mathrm{s}} = 48$ kHz. All DM resonance frequencies that can be observed in Fig. 6(a) are less than 90% of the switching frequency, which is in accordance with the design procedure presented in Section III. The calculations do not consider parasitic components, e.g., winding capacitances, which are found to deteriorate the filter attenuations at frequen-

[2] It is not necessary to introduce a safety factor for $L_{\mathrm{cm},1}$ due to different material properties.

[3] $483\ \mathrm{cm}^3$ is the measured boxed volume of all filter components, which differ from the calculated value of $400\ \mathrm{cm}^3$, because each turn, with the wires of the selected wire diameters, requires a certain radius of curvature to be wound around the toroidal core for the CM choke or the middle leg of the E-core for the DM inductor.

[4] For $L_{\mathrm{dm},1}$, which is realized by two inductors, the surface part of the inductor touching the PCB part almost touching the other coil are not included in the calculation of A_{coil}, cf., Fig. 5.

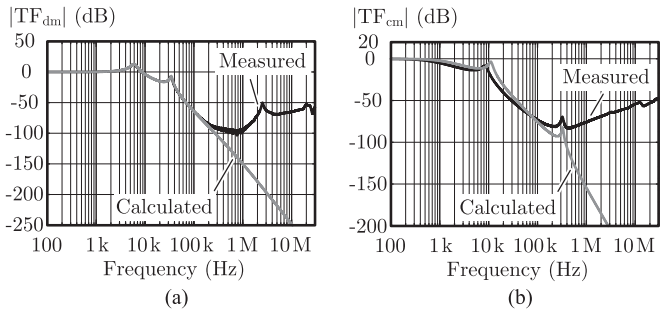

Fig. 6. Measured (black line) and calculated (gray line) transfer functions of the $LCLCL$ EMI input filter for (a) DM and (b) CM.

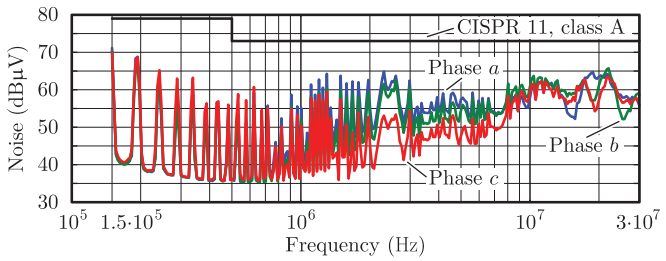

Fig. 7. Measured total (DM + CM) noise spectra of the PWM rectifier system with the realized EMI filter for nominal operation and with $C_{\mathrm{g}} = 25$ nF.

cies greater than ≈ 400 kHz $\ldots$ 500 kHz. The measurements were conducted with a Bode 100 network analyzer (Omicron Lab), the noise floor is reached at -100 dB. Calculated and measured DM transfer functions agree well for frequencies up to 200 kHz (the difference at 192 kHz is 3.5 dB), however, differences are apparent for the CM transfer functions, which, for frequencies below 100 kHz, are addressed to the reduced permeability and increased loss component (associated with the imaginary part of the permeability) of the employed nanocrystalline core material with higher frequencies. At frequencies greater than 100 kHz, the parasitic couplings between the filter stages due to the geometrical arrangement of the components on the PCB cause additional differences between the measured and calculated value of $|\mathrm{TF}_{\mathrm{cm}}|$ (at 192 kHz the difference is 9 dB). Since the envelope of the EMI noise source spectrum is proportional to $1/f$, certain reductions of the attenuations of the EMI filter can be accepted for frequencies above 200 kHz and the filtered EMI noise spectrum still complies with the requirements of CISPR 11. Furthermore, 15 dB margins have been added to the filter's CM and DM attenuations, to take components' tolerances into consideration. For these reasons and with the measured transfer functions of Fig. 6, the EMI filter is expected to be capable to fulfill the requirements for conducted EMI.

Fig. 7 depicts the measured levels of conducted EMI at the mains terminals for all three phases. In the course of this measurement, a 50 µm thick µ-metal plate has been placed between the inductors of the two filter stages to reduce the parasitic magnetic coupling between the stages, which would lower the filter attenuations. Due to the considered margins for the CM and DM attenuations, the obtained filter attenuation is approximately 10 dB greater than needed, since the filter components have been carefully adjusted with respect to the required values. The greatest amplitude of the spectral EMI noise component occurs at 3×48 kHz $= 144$ kHz (instead of 192 kHz), by reason of the test receiver's resolution bandwidth of 9 kHz, which can be mitigated with a slight reduction of the switching frequency, e.g., to 47 kHz.

V. Conclusion

This letter summarizes a systematic approach for the volume optimization of a two-stage DM and CM EMI filter for a 10 kW three-phase, three-level PWM rectifier system. The design approach reveals that most component values are not available for optimization by reason of predefined, practice-oriented boundary conditions, and hence, essentially the ratio $k_{\mathrm{L}} = L_{\mathrm{cm},1}/L_{\mathrm{dm},1}$ is the remaining degree of freedom for the optimization. The optimization procedure detailed in the paper computes a flat minimum of the filter volume for $10 < k_{\mathrm{L}} < 40$. The selected design employs $k_{\mathrm{L}} = 18$ and the corresponding sum of the volumes of all filter components is 483 cm^3 (29.5 in^3). Experimental results verify the effectiveness of the optimized EMI filter, which achieves a boxed volume of 763 cm^3 (46.6 in^3) and a filter power density of 13.1 kW/dm^3 (215 W / in^3). Finally, it should be highlighted that, differently to the DM inductor, the CM inductor is not sufficiently characterized by the phase current and the inductance value; the CM inductor also needs to be designed with respect to the CM voltage-time area generated by the investigated rectifier in order to avoid saturation of its core, and with this, the volume of the CM inductor can be estimated.

References

[1] A. Anthon, Z. Zhang, M. A. E. Andersen, D. G. Holmes, B. McGrath, and C. A. Teixeira, "The benefits of SiC MOSFETs in a T-type inverter for grid-tie applications," *IEEE Trans. Power Electron.*, to be published.

[2] R. Inzunza, R. Okuyama, T. Tanaka, and M. Kinoshita, "Development of a 1500VDC photovoltaic inverter for utility-scale PV power plants," in *Proc. IEEE 2nd Int. Future Energy Electron. Conf.*, 2015, pp. 1–4.

[3] Y. Fang, S. Cao, Y. Xie, and P. Wheeler, "Study on bidirectional-charger for electric vehicle applied to power dispatching in smart grid," in *Proc. IEEE 8th Int. Power Electron. Motion Control Conf.*, 2016, pp. 2709–2713.

[4] Q. Ji, X. Ruan, and Z. Ye, "The worst conducted EMI spectrum of critical conduction mode boost PFC converter," *IEEE Trans. Power Electron.*, vol. 30, no. 3, pp. 1230–1241, Mar. 2015.

[5] D. O. Boillat, F. Krismer, and J. W. Kolar, "Design space analysis and ρ-η Pareto optimization of LC output filters for switch-mode AC power sources," *IEEE Trans. Power Electron.*, vol. 30, no. 12, pp. 6906–6923, Dec. 2015.

[6] N. Zhu, J. Kang, D. Xu, B. Wu, and Y. Xiao, "An integrated AC choke design for common-mode current suppression in neutral-connected power converter systems," *IEEE Trans. Power Electron.*, vol. 27, no. 3, pp. 1228–1236, Mar. 2012.

[7] Y. Levron, H. Kim, and R. W. Erickson, "Design of EMI filters having low harmonic distortion in high-power-factor converters," *IEEE Trans. Power Electron.*, vol. 29, no. 7, pp. 3403–3413, Jul. 2014.

[8] F. Luo, D. Dong, D. Boroyevich, P. Mattavelli, and S. Wang, "Improving high-frequency performance of an input common mode EMI filter using an impedance-mismatching filter," *IEEE Trans. Power Electron.*, vol. 29, no. 10, pp. 5111–5115, Oct. 2014.

[9] R. W. Erickson and D. Maksimovic, *Fundamentals of Power Electronics*, 2nd ed. Norwell, MA, USA: Kluwer, 2001, p. 881.

[10] D. O. Boillat, J. W. Kolar, and J. Mühlethaler, "Volume minimization of the main DM/CM EMI filter stage of a bidirectional three-phase three-level PWM rectifier system," in *Proc. IEEE Energy Convers. Congr. Expo.*, 2013, pp. 2008–2019.

[11] *IEC Standard Voltages*, International Electrotechnical Commission (IEC) Std. IEC 60038, Ed. 7.0, 2009.

[12] J. W. Kolar, U. Drofenik, J. Miniböck, and H. Ertl, "A new concept for minimizing high-frequency common-mode EMI of three-phase PWM rectifier systems keeping high utilization of the output voltage," in *Proc. IEEE 15th Appl. Power Electron. Conf. Expo.*, 2000, vol. 1, pp. 519–527.

[13] J. W. Kolar, "VIENNA Rectifier: Entwicklung und Analyse neuer netzrückwirkungsarmer Dreiphasen-Pulsgleichrichtersysteme (in German)," Ph.D. dissertation, Vienna Univ. Technol., Vienna, Austria, 1998, p. 183.

[14] D. O. Boillat, "Modular high bandwidth switch-mode three-phase AC voltage source," Ph.D. dissertation, ETH Zurich, Zurich, Switzerland, 2016, p. 409.

[15] I. Takahashi, A. Ogata, H. Kanazawa, and A. Hiruma, "Active EMI filter for switching noise of high frequency inverters," in *Proc. Power Convers. Conf.*, 1997, vol. 1, pp. 331–334.

[16] A. L. Julian, G. Oriti, and T. A. Lipo, "Elimination of common-mode voltage in three-phase sinusoidal power converters," *IEEE Trans. Power Electron.*, vol. 14, no. 5, pp. 982–989, Sep. 1999.

[17] S. Ogasawara, H. Ayano, and H. Akagi, "An active circuit for cancellation of common-mode voltage generated by a PWM inverter," *IEEE Trans. Power Electron.*, vol. 13, no. 5, pp. 835–841, Sep. 1998.

[18] *Nanocrystalline VITROPERM EMC Products, PKB-EMC Edition, Vacuumschmelze Inc., Hanau, Germany*, 2010, p. 16.

[19] M. L. Heldwein, L. Dalessandro, and J. W. Kolar, "The three-phase common-mode inductor: Modeling and design issues," *IEEE Trans. Ind. Electron.*, vol. 58, no. 8, pp. 3264–3274, Aug. 2011.

[20] K. Venkatachalam, C. R. Sullivan, T. Abdallah, and H. Tacca, "Accurate prediction of ferrite core loss with nonsinusoidal waveforms using only Steinmetz parameters," in *Proc. IEEE Workshop Comput. Power Electron.*, 2002, pp. 36–41.

[21] J. Mühlethaler, J. W. Kolar, and A. Ecklebe, "Loss modeling of inductive components employed in power electronic systems," in *Proc. IEEE 8th Int. Conf. Power Electron.*, 2011, pp. 945–952.

[22] *Nanocrystalline VITROPERM 500F—Toroidal Cores for Common Mode Chokes and EMC Applications*, Vacuumschmelze Inc., Hanau, Germany, 2005, p. 2

[23] S. A. Mulder, "On the design of low profile high frequency transformers," in *Proc. 5th Int. High Freq. Power Convers. Conf.*, 1990, pp. 141–159.

[24] *Powder Core Catalog 2011, Magnetics*, Pittsburgh, USA, 2012, p. 106.

[25] A. Van den Bossche and V. C. Valchev, *Inductors and Transformers for Power Electronics*. Boca Raton, FL, USA, CRC Press, 2005, p. 456.

[26] K. Raggl, T. Nussbaumer, and J. W. Kolar, "Guideline for a simplified differential-mode EMI filter design," *IEEE Trans. Ind. Electron.*, vol. 57, no. 3, pp. 1031–1040, Mar. 2010.

[27] R. M. Burkart, H. Uemura, and J. W. Kolar, "Optimal inductor design for 3-phase voltage-source PWM converters considering different magnetic materials and a wide switching frequency range," in *Proc. Int. Power Electron. Conf.*, 2014, pp. 891–898.